Available online at www.sciencedirect.com

ScienceDirect

Solar Energy 100 (2014) 23–30

SOLAR ENERGY

www.elsevier.com/locate/solener

Characterization of a CZTS thin film solar cell grown by sputtering method

Tara P. Dhakal [a,c,*], Chien–Yi Peng [a,b], R. Reid Tobias [b], Ramesh Dasharathy [b], Charles R. Westgate [a,c]

[a] Center for Autonomous Solar Power (CASP), SUNY-Binghamton, Vestal, NY, United States
[b] Systems Science and Industrial Engineering, SUNY-Binghamton, Binghamton, NY, United States
[c] Department of Electrical and Computer Engineering, SUNY-Binghamton, Binghamton, NY, United States

Received 17 September 2013; received in revised form 13 November 2013; accepted 29 November 2013

Communicated by: Associate Editor Takhir M. Razykov

Abstract

We report the performance of Cu_2ZnSnS_4 (CZTS) thin film solar cell that showed efficiency in the range of 6.2% without an anti-reflection coating. Initially, the CZTS precursor film was co-sputtered using three different targets; copper (Cu), tin sulfide (SnS) and zinc sulfide (ZnS). The Cu target was subjected to DC power, and RF power was used for the SnS and ZnS targets. The as-grown CZTS film was sulfurized in a H_2S/N_2 environment at 525 °C, which re-crystalized the film with grain sizes in the range of 1 μm. Cadmium sulfide (CdS) was used as the n-type layer. Current–voltage (*I–V*), quantum efficiency (QE) and capacitance–voltage (*C–V*) measurements were used to characterize the cell device. The modeling and analysis of QE and CV data showed that a significant portion of the CZTS layer did not contribute to the photo-generation. Optimizing CZTS phase purity, improving QE in the broader wavelength region, and increasing minority carrier lifetime are necessary steps to further improve CZTS device performance.

Keywords: Thin film solar cells; Cu_2ZnSnS_4; Co-sputtering; *I–V*/QE characteristics

1. Introduction

CZTS is an excellent p-type absorber because of its high absorption coefficient and its ideal band gap of 1.5 eV (Seol et al., 2003; Rajeshmon et al., 2011). A typical CZTS hetero-junction solar cell starts with molybdenum (Mo) as a back contact, CZTS as p-type absorber and CdS as n-type window layer. Highly resistive, intrinsic zinc oxide (i-ZnO) is placed between the transparent conducting oxide (TCO) layer and the window layer to prevent any shunting paths through the n-type layer. Aluminum doped zinc oxide (AZO) (Dhakal et al., 2012a) and tin-doped indium oxide (ITO) (Yang et al., 2008) are used as TCO layers. Silver/chromium (Ag/Cr) is used as finger electrodes.

In recent years, interest in CZTS has increased exponentially since this compound is very similar to the well-studied high efficiency copper indium gallium selenide (CIGS). CZTS differs from CIGS in that it replaces the indium and gallium by less expensive and earth abundant zinc and tin, respectively. However, the highest efficiency observed so far is only 8.4% for the CZTS/CdS hetero-junction (Shin et al., 2013) compared to 20% efficiency for CIGS/CdS hetero-structure (Jackson et al., 2011). According to the widely accepted Shockley–Queisser limit, an efficiency of 28% is possible with the CZTS solar cell (Shockley and Queisser, 1961). In order to achieve efficiencies closer to this limit, there are major challenges that need to be addressed.

* Corresponding author.
E-mail address: tdhakal@binghamton.edu (T.P. Dhakal).

0038-092X/$ - see front matter © 2013 Elsevier Ltd. All rights reserved.
http://dx.doi.org/10.1016/j.solener.2013.11.035

Although it was suggested from the measurement of temperature dependence of open circuit voltage (V_{oc}) that the interface recombination may be a dominant factor for the observed low V_{oc} in CZTSSe devices (Gunawan et al., 2010; Mitzi et al., 2011), a recent study suggests that the important factor limiting CZTSSe solar cell efficiencies is the existence of tail states due to electrostatic potential fluctuations induced by strong compensation (Gokmen et al., 2013). In addition, unlike CIGS, CZTS has a rather small window of thermodynamically stable phase (Chen et al., 2010; Nagoya et al., 2010). A slight variation in the growth parameters favors the formation of secondary phases including Cu_2SnS_3, ZnS, SnS_2 and CuS. First principle calculations have shown that Cu at Zn site are the dominant defects in all possible ranges of CZTS phase stability (Nagoya et al., 2011). Because Cu is a monovalent and zinc is a divalent cation, the Cu antisite (Cu substituted at Zn site) defect acts as an accepter giving rise to p-type conductivity in CZTS. A Cu-poor and Zn-rich CZTS phase is desired to suppress the Cu_{Zn} antisite defects and Zn-poor phases like Cu_2SnS_3. But with Zn-rich composition, formation of the competitive phase such as ZnS occurs. Thus careful control of the Cu and Zn-compositions is necessary.

Another issue that has reduced the efficiency of the CZTS solar cell is high series resistance. The series resistance of a solar cell device depends on the quality of the TCO layer, top electrode, and the electronic nature of the bottom Mo/CZTS contact (Wang et al., 2010). The presence of the MoS_2 layer at the interface between CZTS and Mo back contact could also be responsible for high series resistance in CZTS devices (Mitzi et al., 2011; Scragg et al., 2013). In this article, a detailed performance analysis of CZTS/CdS cell device with an efficiency of 6.2% is reported. A very simple QE modeling is used to show the generation in the CZTS film layer by layer. The cell device is also analyzed by capacitance–voltage (C–V) measurement, an outcome of which has verified QE modeling results. A detailed account of XRD peaks corresponding to CZTS kesterite phase is also presented. The current–voltage (I–V) characteristics of the device were fitted in a single diode model and the extracted parameters were then used to see how lowering series resistance would help to enhance the efficiency. The characterizations are presented in a way to understand the shortcomings of the CZTS solar cell.

2. Experimental

The precursor layer for the CZTS absorber was placed on molybdenum (Mo) coated glass substrate by co-sputtering of Cu, SnS and ZnS. The targets (2.0″ Dia. × 0.125″ Thick) with 99.99% were purchased from Kurt J. Lesker Company. In a typical run, the power used for Cu, SnS and ZnS targets were 35 W DC, 65 W RF and 220 W RF, respectively. This was followed by an annealing of the CZTS layer in H_2S/N_2 (5/95%) environment at atmospheric pressure at 500–525 °C from 3 to 4 h in a tube furnace with quartz tube. This resulted in grain enhancement and near single phase CZTS crystals. The phase purity of the CZTS layer was assessed by X-ray diffraction (XRD) measurement. X-ray Photoelectron Spectroscopy (XPS) measurements were performed using a Versaprobe PHI 5000 scanning ESCA system which employs monochromatic Al Kα X-rays.

Cadmium sulfide (CdS) was used as an n-type layer, which was synthesized using chemical bath deposition. Prior to the deposition of CdS layer, the CZTS surface was etched for two minutes in an 1 M sodium cyanide (NaCN) solution prepared in DI water. Then a thin intrinsic zinc oxide (i-ZnO) layer was coated followed by a transparent conducting oxide (TCO) layer. The thicknesses of CdS, i-ZnO, and TCO were around 60 nm, 50 nm and 300 nm respectively. The fabricated cell structure was Glass/Mo/CZTS/CdS/ZnO/TCO (AZO or ITO)/Cr–Ag.

Carrier concentration of the CZTS film was obtained by Hall Effect measurement. Capacitance–voltage measurements were performed to estimate the acceptor density and the built-in-potential using Keithley's semiconductor characterization system (KTEI V 8.2). I–V characteristics of the cell under 1 sun light were performed in a class AAA solar simulator from Photo Emission Tech. Inc. The quantum efficiency measurement was carried out in a commercial system from PV Measurements, Inc. The absorption data was obtained from a UV–vis spectrophotometer from Angstrom Sun Technologies Inc. Room temperature PL data of the CZTS film was obtained using 532 nm incident laser light at 10 μJ in reflection geometry with an exposure time of 30 s.

3. Results and discussion

3.1. Structural properties

The film crystallinity and the orientation were assessed by θ–2θ X-ray diffraction (XRD) in grazing angle incidence geometry. The angle of incidence used was 0.6°, which was an optimized value to avoid reflection and the substrate peaks. X-ray diffraction patterns shown in Fig. 1 of our CZTS film match almost perfectly with those of the kesterite phase (PDF # 01-075-4122; International Center for Diffraction Data). Although XRD patterns of CZTS are usually compared with data from PDF # 00-026-0575 (Todorov et al., 2010), the reflections from all possible peaks are missing in this pdf data, which may lead to a wrong conclusion on the additional peaks seen in the observed data. The intensity of the XRD patterns is plotted in a smaller scale to see the presence of any impurity peaks. The peaks indicated with the asterisk mark are predominantly due to Mo beneath the CZTS film although CZTS peaks also exist in these locations. The broadness on both sides of the (200)/(004) peak of the CZTS film is due to the peaks from the MoS_2 layer formed between the Mo and CZTS interface. A tiny peak on the left side of the (224) peak is due to the MoS_2 as well. There are a few low

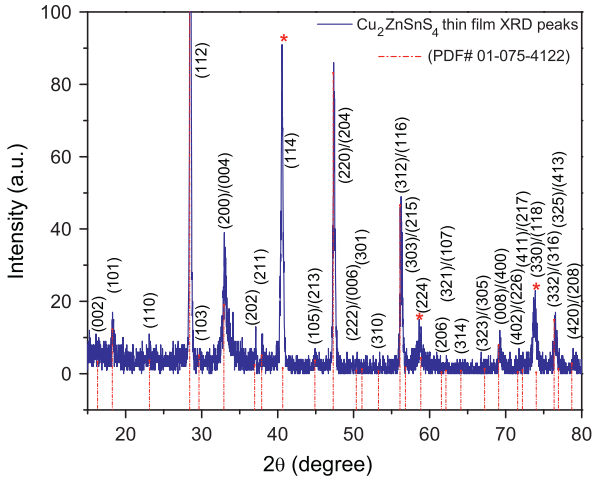

Fig. 1. XRD spectra of the annealed CZTS film.

intensity peaks that do not match with the kesterite phase. They could be from the secondary phases such as SnS (Herzenbergite; PDF: 00-014-0620), SnS_2 (Berndtite; PDF: 00-001-1010) and CuS (Covellite; PDF: 00-002-0820). However, it is difficult to draw a definitive conclusion because of the low signal to noise ratio. The presence of the ZnS phase is a certainty (bright features on SEM images), but the overlap between ZnS (Sphalerite; PDF: 00-001-0792) and CZTS peaks makes is difficult to distinguish them from XRD spectra.

3.2. Composition analysis

Fig. 2 shows an SEM image of the H_2S-annealed CZTS film, and Table 1 shows the corresponding elemental compositions and standard ratios used. An optimal cell device made from this film exhibited 6.21% efficiency. The Cu/(Zn + Sn) and Zn/Sn ratios are desired in the vicinity of 0.8 and 1.2 respectively for optimal cell efficiency (Guo et al., 2010). However, the Cu/(Zn + Sn) and Zn/Sn ratios obtained in our film before etching were 0.79 and 1.58 respectively. These ratios were obtained from the area of the samples with magnifications lower than 500X to represent the overall composition of the film, shown in "overall" column in Table 1. The bright spots in Fig. 2 are probably ZnS precipitates because the EDS data showed significantly higher zinc concentration. The EDS analysis performed on the dark regions showed less zinc (cf. "Dark region" column of Table 1). The ratios were similar after NaCN etching, although the amounts of Cu and Zn are slightly reduced. The amount of Cu/Zn reduction is greater in the dark/overall region. Please note that species rich in Cu appear darker and the species that are rich in zinc appear brighter in SEM image. Although the reports on optimal Cu/(Zn + Sn) and Zn/Sn ratios vary, it appears that Zn-rich and Cu-poor compositions are desired for better performance in CZTS solar cells (Ennaoui et al., 2009; Tanaka et al., 2009).

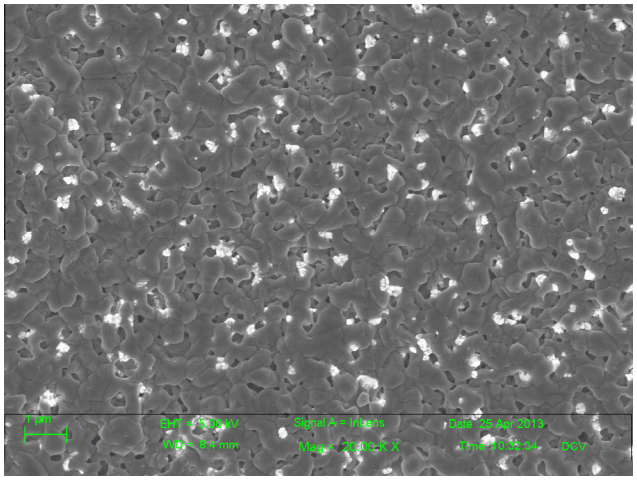

Fig. 2. SEM image of the CZTS film.

To improve the quality of the absorber–emitter interface, a preferential etching of the secondary phases present in the CZTS surface was performed before forming the n-type CdS layer. A soft XPS study confirmed the absence of unwanted secondary phases, at least at the interface. The soft XPS data obtained on the etched bare Cu-poor sample showed less Zn 3*d* and Cu $2p_{3/2}$ intensities compared to the untouched case. This shows that the Cu oxide and sulfide may have been removed along with Cu-free species such as $ZnSnS_3$ (or a mixture of ZnS and SnS_2 since XPS alone cannot distinguish it) (Bär et al., 2012). The devices made with etching of the CZTS surface had efficiency almost twice as high as those made without etching. Etching was used for the device with 6.2% efficiency. Whether the etching gave rise to the electrically benign character at the CZTS/CdS interface similar to what is observed in CIGS devices (Chen et al., 2010) is a matter that requires further investigation.

3.3. Optical properties

The absorption coefficient calculated using the transmittance and reflectance data was higher than 5×10^4 cm^{-1} in most of the visible region (Fig. 3a). The band gap derived using a Tauc plot (Tauc et al., 1966; Dhakal et al., 2012b) was 1.52 eV which matched with the effective band gap of 1.53 eV assessed by the inflection point of the internal quantum efficiency (IQE) graph (Todorov et al., 2013). The inflection point corresponds to the maximum of *dIQE/dE* (Fig. 3c). However, the peak of the photoluminescence (PL) of the CZTS film excited with 532 nm incident laser light at 10 μJ for 30 s was at 1.35 eV (Fig. 3d). This difference is attributed to the presence of a conduction band to impurity radiative recombination channel contributing to the PL signal and also to the inhomogeneity in the sample in which the luminescence at low energy is more dominant (Todorov et al., 2013). The data observed from Tauc plot and QE data is an average of the overall sample.

Table 1
Elemental composition of the annealed CZTS thin films before and after etching.

Elements	Overall (un-etched) (At.%)	Overall (etched) (At.%)	Dark region (un-etched) (At.%)	Dark region (etched) (At.%)
S	47.91	49.83	49.25	51.03
Sn	11.31	11.34	12.05	11.81
Cu	22.96	22.23	24.07	22.60
Zn	17.82	16.61	14.62	14.57
Cu/(Zn + Sn)	0.79	0.80	0.90	0.86
Zn/Sn	1.58	1.47	1.21	1.23
Cu/Sn	2.03	1.96	1.99	1.91

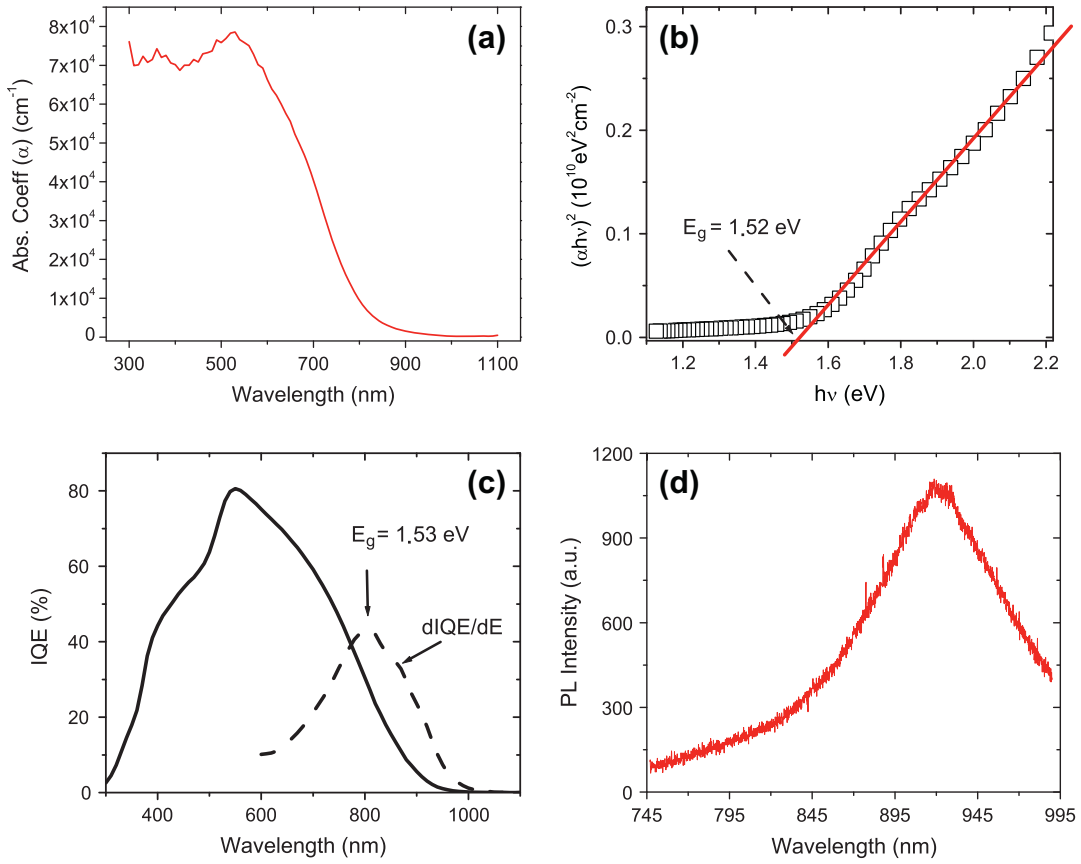

Fig. 3. (a) Absorption coefficient of the CZTS film, (b) Tauc plot for band gap measurement, (c) inflection point of IQE graph showing the effective band gap, and (d) PL spectrum.

Nonetheless, the band gap and the absorption coefficient are optimal for photo-energy conversion.

3.4. Electrical properties

Fig. 4 shows the *I–V* graph of the optimal cell device. The efficiency of the cell is 6.2%. The open circuit voltage (V_{oc}) is 603 mV and the short circuit current is 19 mA/cm^2. The series (R_s) and shunt (R_{sh}) resistances are 5.61 Ωcm^2 and 400 Ωcm^2 respectively. The fill factor (FF) is 55%. The low R_{sh} can be attributed to the defective CZTS layer as shown in the cross-sectional SEM image of Fig. 5. The bright spots of ZnS appear to be precipitated more on the bottom than on the surface (cf. Fig. 2 and 5). It is difficult to avoid ZnS precipitation, since it is one of the competing phases in Zn-rich CZTS phase formation (Nagoya et al., 2011). The R_{sh} of the cell can be increased by improving the material properties of the absorber layer. On the other hand, R_s of the cell is relatively higher. Using single diode modeling (Carrero et al., 2011; Kim and Choi, 2010), we found that an increase of efficiency close to 1% is possible if the series resistance is reduced to 10% of its current value. This is experimentally achievable by improving the TCO layer as well as the back contact. In addition to the suboptimal conductivity of the TCO, the presence of MoS_2 layer at the interface could be responsible for high series resistance in the CZTS device. As shown in Fig. 5, a 60 nm thick MoS_2 layer is formed.

The competitive efficiencies of CZTS/CdS solar cell with CZTS precursor layer grown by sputtering stand at 6.7% by Katagiri et al. (Hironori et al., 2008) and 6.3% by Solar Frontier (Homare et al., 2013), although an efficiency of

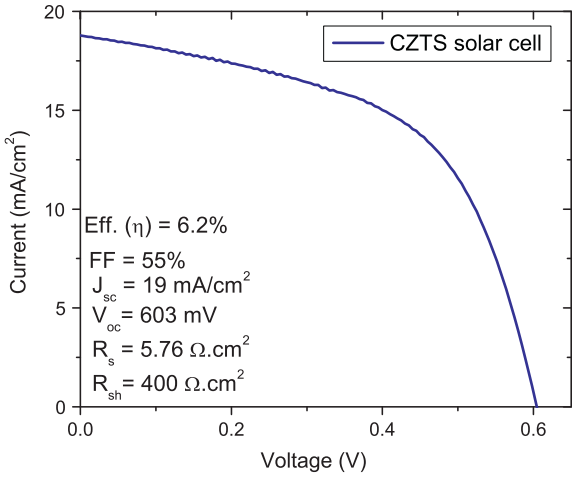

Fig. 4. *I–V* graph of the CZTS solar cell.

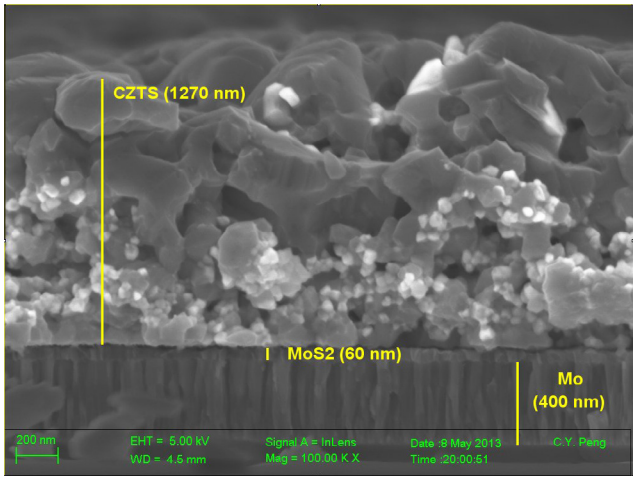

Fig. 5. Cross-sectional SEM image of the CZTS layer grown on Mo-coated glass substrate.

9.2% has been recently reported by Solar Frontier for CZTS with hybrid (CdS + InS) n-type layer instead of just CdS layer (Homare et al., 2013). The cell efficiency of 6.2% reported here is for the cell without anti-reflection (AR) coating with which an increase of at least 0.5% can be safely assumed. In addition, if the cells were fabricated in an in-line type of vacuum system, the efficiency of the cell will improve further. Thus our cells are on par with, if not better than, the competitive CZTS/CdS cell devices reported by Katagiri et al. and Solar Frontier for CZTS precursor grown by sputtering methods. It should be noted here that efficiencies beyond 8% have been reported for CZTS/CdS devices if the CZTS layer is grown by evaporation of metal precursors (Shin et al., 2013).

3.5. Quantum efficiency

External quantum efficiency (EQE) as a function of wavelength was measured (Fig. 6a). The maximum EQE is about 70%. The reflectance (R) was also measured for the whole device to estimate internal quantum efficiency (IQE). The cell device has reflection in the range from 15% to 17%. After taking the reflection factor out, the internal quantum efficiency (IQE = EQE/1−R) is roughly 80%. The short circuit current density (J_{sc}) can be estimated by using the following formula:

$$J_{sc} = q \int \Phi(\lambda) \mathrm{QE}(\lambda) d\lambda \quad (1)$$

where $\Phi(\lambda)$ is the incident photon flux, and q is the electronic charge. The current estimated from EQE and IQE graph by using Eq. (1) shows that an increase of 2.5 mA/cm^2 is possible if the reflectance were zero. This corresponds to an approximate increase of 1% in cell efficiency, but this is a limit since zero reflectance is practically impossible. A preliminary study performed by capping our lower efficiency (~4–5%) cells by an AR coating showed an efficiency increase between 0.5% and 0.6%. Thus with AR coating this cell with 6.2% is expected to be at least 6.7%.

Quantum efficiency data was fitted with a simple model (Fig. 6b). In this model, the global AM 1.5 spectrum [ASTM G173-03 Reference Spectra] is used as input photon flux. The generation of the carriers is based on the absorbed photons with an assumption that all the absorbed photons are used to generate the carriers. The CZTS layer is divided into several layers of 70 nm thickness and the generation in each layer is modeled. The generation in the first layer is the total absorption in the first layer multiplied by the incident photons. Then the generation in the next layer is the total absorption in the next layer multiplied by the transmitted photons from the first layer, where the transmitted photon spectrum is given by

$$\begin{aligned}&\text{Transmitted spectrum}\\ &\quad = 1 - \text{reflected spectrum}\\ &\qquad - \text{total absorption of the previous layer}\end{aligned} \quad (2)$$

The absorption is experimentally measured, but the reflected spectrum is obtained by using the Fresnel cavity reflectivity formula (Eugene, 2001). If the refractive indices of the incident and reflected medium are known, the reflected spectrum can be calculated. This way the carrier generation can be simulated for any number of layers with any thickness.

Fig. 6b shows the best fit to the QE data using this simple model, which has regions (shaded part in the figure) not accounted for by the model around red region of the spectrum. This shows that a significant portion of the CZTS is not contributing to the photo-generation. Note that the 8th layer and the remaining 740 nm layer are not contributing at all. The 6th and 7th layers are only generating 70% and 60% respectively. During the fitting, these values of collection efficiencies can be chosen until a best fit is obtained. As we know zinc-rich and copper-poor phase of CZTS are good for photo-generation (Nagoya et al., 2011). So, it is possible that a good portion of the CZTS layer may have a CZTS phase with less than optimum composition. The

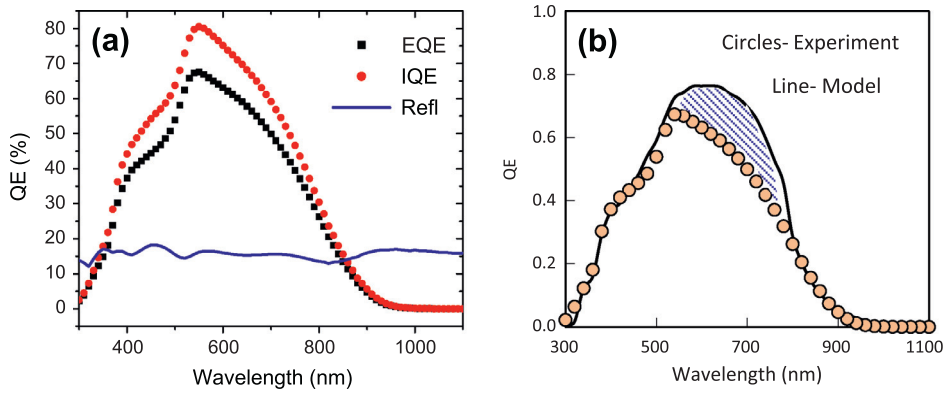

Fig. 6. (a) External quantum efficiency (EQE), internal quantum efficiency (IQE) and reflectance of the CZTS solar cell. (b) External quantum efficiency data fitted with a model.

Table 2
Fractional generation from various CZTS layers of the 6.2% cell device.

CZTS layer	1st	2nd	3rd	4th	5th	6th	7th	8th	Remainder
Layer thickness (nm)	70	70	70	70	70	70	70	70	740
Total thickness (nm)	70	140	210	280	350	420	490	560	1300
Collection efficiency	1	1	1	1	1	0.7	0.6	0	0
Fractional generation	35%	23%	16%	11%	8%	4%	3%	0%	0%

CZTS layer used in the cell was 1.3 μm thick. With the best fit, we could estimate that only the first 450 nm contributed to the photo-generation (please see Table 2 for the fractional generation of various layers). In spite of the simplicity of the model, it helped us to realize that a significant amount within the CZTS layer was not being used for photo-conversion. Thus an optimization of the annealing process to achieve a single phase CZTS that contributes to the photo-generation is a must to improve beyond the current efficiency of the CZTS cell.

3.6. Capacitance–voltage (C–V) measurements

C–V measurements carried out revealed more fundamental properties of the device to pave the way toward achieving a much higher efficiency. Doping density and built-in-voltage at the cell junction were derived from $1/C^2$ vs. V plot of *C–V* data according to the following relations (Tripathi and Sharma, 2012; Yakuphanoglu, 2011):

$$\frac{1}{C^2} = \frac{2}{qN_a\varepsilon_o\varepsilon_s A^2}(V_{bi} - V) \tag{3}$$

$$N_a = \frac{2}{q\varepsilon_o\varepsilon_s A^2\left[\frac{d}{dV}(1/C^2)\right]} \tag{4}$$

where N_a = doping density ($1/cm^3$), q = the electron charge (1.60219×10^{-19} *C*), ε_o = permittivity of free space (8.85×10^{-14} F/cm), ε_s = dielectric constant (ε_s of *CZTS* = 7 (Zhao and Persson, 2011)), A = area of the cell (cm^2), C = measured capacitance and V = applied DC voltage.

From Eqs. (3) and (4), we see that the built-in-potential (V_{bi}) and the doping density can be obtained from the intercept and slope of line in $1/C^2$ vs. V plot as shown in Fig. 7 below. The V_{bi} was 0.67 V, slightly higher than the V_{oc} for this device. The doping density (N_a) calculated using Eq. (4) was $5.75 \times 10^{16}/cm^3$, which was very close to the carrier (hole) density ($5.65 \times 10^{16}/cm^3$) measured for the CZTS film using Hall Effect measurement. With V_{bi} and N_a, the depletion width (W_d) estimated using the relation, $W_d = (2\varepsilon_o\varepsilon_s V_{bi}/qN_a)^{1/2}$ (Shin et al., 2013) was 95 nm.

The carrier diffusion length was also estimated using the following relation:

$$L_n \sim \sqrt{D_n\tau} = \sqrt{\mu_n \frac{kT}{q}\tau} \tag{5}$$

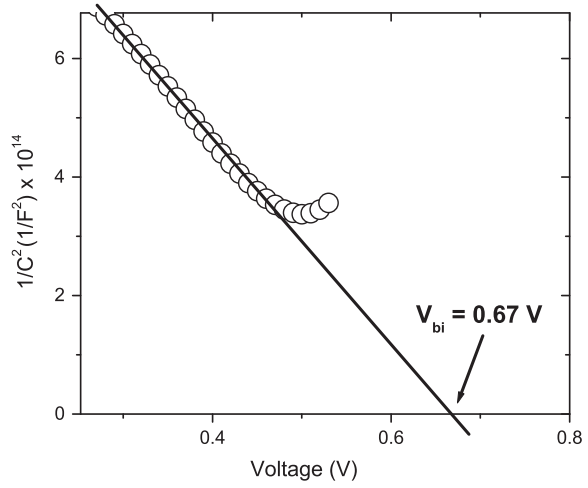

Fig. 7. $1/C^2$ vs. V plot obtained from *C–V* measurement.

where D_n is the diffusivity of electrons, μ_n is electron mobility, τ is minority carrier lifetime and kT/q is thermal voltage at room temp (25.85 mV). The Hall mobility of the CZTS film was 15 cm^2/V s. Since the Hall mobility values reported in the literature are 6 to 30 cm^2/V s (Shin et al., 2013), we have used the lowest value of 6 cm^2/V s for electron mobility. τ is estimated to be 8 ns as reported by Shin et al. (2013). With these values the carrier diffusion length calculated from Eq. (5) was 350 nm. This is the average distance the electrons can travel toward the edge of the space charge region before recombining. Thus the total thickness contributing to the photocurrent is L_n (350 nm) + W_d (95 - nm) = 445 nm. This is in agreement with the thickness value of 450 nm obtained earlier from QE modeling.

4. Conclusions

A 6.2% efficient CZTS/CdS solar cell device was fabricated using co-sputtering followed by H_2S annealing. The CZTS film showed the kesterite phase, although minor impurity phases were observed. The EDS analysis showed Cu-poor and Zn-rich compositions. The maximum internal quantum efficiency of the cell was 80%. QE modeling and *C–V* measurement confirmed that only 450 nm thickness of the CZTS film was contributing to the photo-generation. Our future work would be an optimization of the CZTS film for phase purity.

Acknowledgements

This study was supported by the Office of Naval Research; Grant No. N00014-11-1-0658. The authors would also like to thank Prof. Angus Rockett of University of Illinois at Urbana-Champaign for QE modeling discussion and Prof. Louis Piper, Prof. Joon Jang, Prof. Bruce White and Prof. David Klotzkin of Binghamton University for XPS, PL, *C–V* and AR coating measurements respectively. TD also would like to thank Daniel Vanhart for his support with SEM imaging.

References

Bär, M., Schubert, B.-., Marsen, B., Wilks, R.G., Blum, M., Krause, S., Pookpanratana, S., Zhang, Y., Unold, T., Yang, W., Weinhardt, L., Heske, C., Schock, H., 2012. Cu_2ZnSnS_4 thin-film solar cell absorbers illuminated by soft X-rays. J. Mater. Res. 27, 1097–1104.

Carrero, C., Ramírez, D., Rodríguez, J., Platero, C.A., 2011. Accurate and fast convergence method for parameter estimation of PV generators based on three main points of the *I–V* curve. Renew. Energy 36, 2972–2977.

Chen, S., Yang, J., Gong, X.G., Walsh, A., Wei, S., 2010. Intrinsic point defects and complexes in the quaternary kesterite semiconductor Cu_2ZnSnS_4. Phys. Rev. B 81, 245204.

Dhakal, T., Nandur, A.S., Christian, R., Vasekar, P., Desu, S., Westgate, C., Koukis, D.I., Arenas, D.J., Tanner, D.B., 2012a. Transmittance from visible to mid infra-red in AZO films grown by atomic layer deposition system. Sol. Energy 86, 1306–1312.

Dhakal, T., Vanhart, D., Christian, R., Nandur, A., Sharma, A., Westgate, C.R., 2012b. Growth morphology and electrical/optical properties of Al-doped ZnO thin films grown by atomic layer deposition. J. Vac. Sci. Technol. A 30, 021202.

Ennaoui, A., Lux-Steiner, M., Weber, A., Abou-Ras, D., Kötschau, I., Schock, H.-., Schurr, R., Hölzing, A., Jost, S., Hock, R., Voß, T., Schulze, J., Kirbs, A., 2009. Cu_2ZnSnS_4 thin film solar cells from electroplated precursors: Novel low-cost perspective. Thin Solid Films 517, 2511–2514.

Eugene, H., 2001. Optics. In: fourth ed. Pearson Education.

Gokmen, T., Gunawan, O., Todorov, T.K., Mitzi, D.B., 2013. Band tailing and efficiency limitation in kesterite solar cells. Appl. Phys. Lett., 103.

Gunawan, O., Todorov, T.K., Mitzi, D.B., 2010. Loss mechanisms in hydrazine-processed $Cu_2ZnSn(Se, S)_4$ solar cells. Appl. Phys. Lett. 97, 233506.

Guo, Q., Ford, G.M., Yang, W., Walker, B.C., Stach, E.A., Hillhouse, H.W., Agrawal, R., 2010. Fabrication of 7.2% efficient cztsse solar cells using CZTS nanocrystals. J. Am. Chem. Soc. 132, 17384–17386.

Hironori, K., Kazuo, J., Satoru, Y., Tsuyoshi, K., Win, S.M., Tatsuo, F., Tadashi, I., Tomoyoshi, M., 2008. Enhanced conversion efficiencies of Cu_2ZnSnS_4-based thin film solar cells by using preferential etching technique. Appl. Phys. Express 1, 041201.

Homare, H., Noriyuki, S., Takuya, K., Hiroki, S., 2013. High Voltage Cu2ZnSnS4 Submodules by Hybrid Buffer Layer. In: 39th IEEE Photovoltaic Specialists Conference

Jackson, P., Hariskos, D., Lotter, E., Paetel, S., Wuerz, R., Menner, R., Wischmann, W., Powalla, M., 2011. New world record efficiency for Cu(In, Ga)Se_2 thin-film solar cells beyond 20%. Prog. Photovoltaics Res. Appl. 19, 894–897.

Kim, W., Choi, W., 2010. A novel parameter extraction method for the one-diode solar cell model. Sol. Energy 84, 1008–1019.

Mitzi, D.B., Gunawan, O., Todorov, T.K., Wang, K., Guha, S., 2011. The path towards a high-performance solution-processed kesterite solar cell. Sol. Energ. Mater. Sol. Cells 95, 1421–1436.

Nagoya, A., Asahi, R., Wahl, R., Kresse, G., 2010. Defect formation and phase stability of Cu_2ZnSnS_4 photovoltaic material. Phys. Rev. B 81, 113202.

Nagoya, A., Asahi, R., Kresse, G., 2011. First-principles study of Cu_2ZnSnS_4 and the related band offsets for photovoltaic applications. J. Phys.: Condens. Matter 23, 404203.

Rajeshmon, V.G., Kartha, C.S., Vijayakumar, K.P., Sanjeeviraja, C., Abe, T., Kashiwaba, Y., 2011. Role of precursor solution in controlling the opto-electronic properties of spray pyrolysed Cu_2ZnSnS_4 thin films. Sol. Energy 85, 249–255.

Scragg, J.J., Kubart, T., WÃ¤tjen, J.T., Ericson, T., Linnarsson, M.K., Platzer–BjÃ¶rkman, C., 2013. Effects of back contact instability on Cu_2ZnSnS_4 devices and processes. Chem. Mater. 25, 3162–3171.

Seol, J., Lee, S., Lee, J., Nam, H., Kim, K., 2003. Electrical and optical properties of Cu_2ZnSnS_4 thin films prepared by rf magnetron sputtering process. Sol. Energy Mater. Sol. Cells 75, 155–162.

Shin, B., Gunawan, O., Zhu, Y., Bojarczuk, N.A., Chey, S.J., Guha, S., 2013. Thin film solar cell with 8.4% power conversion efficiency using an earth-abundant Cu_2ZnSnS_4 absorber. Prog. Photovoltaics Res. Appl. 21, 72–76.

Shockley, W., Queisser, H.J., 1961. Detailed balance limit of efficiency of p–n junction solar cells. J. Appl. Phys. 32, 510–519.

Tanaka, K., Oonuki, M., Moritake, N., Uchiki, H., 2009. Thin film solar cells prepared by non-vacuum processing. Sol. Energy Mater. Sol. Cells 93, 583–587.

Tauc, J., Grigorovici, R., Vancu, A., 1966. Optical properties and electronic structure of amorphous germanium. Phys. Status Solidi B 15, 627–637.

Todorov, T.K., Reuter, K.B., Mitzi, D.B., 2010. High-efficiency solar cell with earth-abundant liquid-processed absorber. Adv. Mater. 22, E156–E159.

Todorov, T.K., Tang, J., Bag, S., Gunawan, O., Gokmen, T., Zhu, Y., Mitzi, D.B., 2013. Beyond 11% efficiency: characteristics of state-of-the-art $Cu_2ZnSn(S, Se)_4$ solar cells. Adv. Energy Mater. 3, 34–38.

Tripathi, S.K., Sharma, M., 2012. Analysis of the forward and reverse bias *I–V* and *C–V* characteristics on Al/PVA:n-PbSe polymer nanocomposites Schottky diode. J. Appl. Phys. 111, 074513.

Wang, K., Gunawan, O., Todorov, T., Shin, B., Chey, S., Bojarczuk, N., Mitzi, D., Guha, S., 2010. Thermally evaporated Cu_2ZnSnS_4 solar cells. Appl. Phys. Lett. 97, 143508–143508–3.

Yakuphanoglu, F., 2011. Nanostructure Cu_2ZnSnS_4 thin film prepared by sol–gel for optoelectronic applications. Sol. Energy 85, 2518–2523.

Yang, C., Lee, S., Lin, T., Chen, S., 2008. Electrical and optical properties of indium tin oxide films prepared on plastic substrates by radio frequency magnetron sputtering. Thin Solid Films 516, 1984–1991.

Zhao, H., Persson, C., 2011. Optical properties of Cu(In, Ga)Se_2 and $Cu_2ZnSn(S, Se)_4$. Thin Solid Films 519, 7508–7512.